Supplementary Material for

Projection to extract the perpendicular component (PEPC) method for extracting kinetics from time-resolved data

H. Ki,[1,2] J. Gu,[1,2] Y. Cha,[1,2] K. W. Lee,[1,2] and H. Ihee[1,2,a]

[1]Department of Chemistry and KI for the BioCentury, Korea Advanced Institute of Science and Technology (KAIST), Daejeon, 34141, Republic of Korea

[2]Center for Advanced Reaction Dynamics, Institute for Basic Science, Daejeon, 34141, Republic of Korea

[a] E-mail: hyotcherl.ihee@kaist.ac.kr

This PDF file includes:
  Supplementary Discussions
  Supplementary Figures
  Supplementary References

I. Supplementary Discussions

A. Mathematical background for the decomposition of SADS$_k$ into SADS$_{k,\parallel}$ and SADS$_{k,\perp}$

An arbitrary vector x as well as SADS$_{k,\parallel}$ can be mathematically decomposed into two components, a component $x_{\parallel}$ that is on the plane spanned by two vectors, $(\partial S/\partial T)_\rho$ and $(\partial S/\partial \rho)_T$, and the other component $x_{\perp}$ that is in the direction perpendicular to this plane. Because SADS$_{k,\parallel}$ is on the plane spanned by $(\partial S/\partial T)_\rho$ and $(\partial S/\partial \rho)_T$, SADS$_{k,\parallel}$ can be expressed as a linear combination of $(\partial S/\partial T)_\rho$ and $(\partial S/\partial \rho)_T$. The coefficients of the linear combination for SADS$_{k,\parallel}$, $d_{k,T}$ and $d_{k,\rho}$, can be calculated through the following arithmetic process without fitting. First, $(\partial S/\partial T)_\rho$ can be decomposed into two components, one parallel to $(\partial S/\partial \rho)_T$ and the other perpendicular to $(\partial S/\partial \rho)_T$. Let's denote the former and latter components as $(\partial S/\partial T)_{\rho,\parallel}$ and $(\partial S/\partial T)_{\rho,\perp}$, respectively. Then, the two components can be expressed as follows:

$$(\partial S/\partial T)_{\rho,\parallel} = [(\partial S/\partial T)_\rho \cdot (\partial S/\partial \rho)_T / |(\partial S/\partial \rho)_T|] \times (\partial S/\partial \rho)_T / |(\partial S/\partial \rho)_T|, \tag{S1}$$

$$(\partial S/\partial T)_{\rho,\perp} = (\partial S/\partial T)_\rho - (\partial S/\partial T)_{\rho,\parallel}, \tag{S2}$$

where $\cdot$ denotes the inner product of the vectors, $|A|$ denotes the norm of the vector A and $\times$ denotes a scalar multiplication. In the same way, $(\partial S/\partial \rho)_T$ can be decomposed into two components as follows:

$$(\partial S/\partial \rho)_{T,\parallel} = [(\partial S/\partial \rho)_T \cdot (\partial S/\partial T)_\rho / |(\partial S/\partial T)_\rho|] \times (\partial S/\partial T)_\rho / |(\partial S/\partial T)_\rho|, \tag{S3}$$

$$(\partial S/\partial \rho)_{T,\perp} = (\partial S/\partial \rho)_T - (\partial S/\partial \rho)_{T,\parallel}. \tag{S4}$$

Substituting the above expressions into Eq. (15) in the main text, we get:

$$\begin{aligned}
\text{SADS}_k(q) &= d_{k,T} \times (\partial S/\partial T)_\rho + d_{k,\rho} \times (\partial S/\partial \rho)_T + \text{SADS}_{k,\perp}(q) \\
&= d_{k,T} \times [(\partial S/\partial T)_{\rho,\parallel} + (\partial S/\partial T)_{\rho,\perp}] + d_{k,\rho} \times (\partial S/\partial \rho)_T \\
&\quad + \text{SADS}_{k,\perp}(q) \\
&= d_{k,T} \times (\partial S/\partial T)_{\rho,\perp} + [d_{k,T} \times ((\partial S/\partial T)_\rho \cdot (\partial S/\partial \rho)_T / |(\partial S/\partial \rho)_T|^2 \\
&\quad + d_{k,\rho})] \times (\partial S/\partial \rho)_T + \text{SADS}_{k,\perp}(q) \\
&= d_{k,T} \times (\partial S/\partial T)_\rho + d_{k,\rho} \times [(\partial S/\partial \rho)_{T,\parallel} + (\partial S/\partial \rho)_{T,\perp}] \\
&\quad + \text{SADS}_{k,\perp}(q) \\
&= [d_{k,T} + d_{k,\rho} \times (\partial S/\partial \rho)_T \cdot (\partial S/\partial T)_\rho / |(\partial S/\partial T)_\rho|^2] \times (\partial S/\partial T)_\rho \\
&\quad + d_{k,\rho} \times (\partial S/\partial \rho)_{T,\perp} + \text{SADS}_{k,\perp}(q)
\end{aligned} \tag{S5}$$

Since $(\partial S/\partial T)_{\rho, \perp} \perp (\partial S/\partial \rho)_T$ and $(\partial S/\partial T)_{\rho, \perp} \perp SADS_{k, \perp}(q)$,

$$SADS_k(q) \cdot (\partial S/\partial T)_{\rho, \perp} = \{d_{k, T} \times (\partial S/\partial T)_{\rho, \perp} + [d_{k, T} \times ((\partial S/\partial T)_\rho$$
$$\cdot (\partial S/\partial \rho)_T/|(\partial S/\partial \rho)_T|^2 + d_{k, \rho})] \times (\partial S/\partial \rho)_T$$
$$+ SADS_{k, \perp}(q)\} \cdot (\partial S/\partial T)_{\rho, \perp} \tag{S6}$$
$$= d_{k, T} \times (\partial S/\partial T)_{\rho, \perp} \cdot (\partial S/\partial T)_{\rho, \perp}$$
$$= d_{k, T} \times |(\partial S/\partial T)_{\rho, \perp}|^2$$

Accordingly, $d_{k, T}$ can be simply calculated as follows:

$$d_{k, T} = SADS_k(q) \cdot (\partial S/\partial T)_{\rho, \perp}/|(\partial S/\partial T)_{\rho, \perp}|^2. \tag{S7}$$

In the same way, $d_{k, \rho}$ can be calculated as follows:

$$d_{k, \rho} = SADS_k(q) \cdot (\partial S/\partial \rho)_{T, \perp}/|(\partial S/\partial \rho)_{T, \perp}|^2. \tag{S8}$$

B. Horizontal stripes in the contour plot of the PEPC-treated data

Upon careful inspection, it may be noticed that there are some horizontal (the direction parallel to the t axis) stripes in the PEPC-treated curves shown in Figs. 2, 3, and 4. We investigated the origin of the horizontal stripes and determined that the artifact was not created by the PEPC process and was already present in the original data, except for the case of Fig. 3(a).

For instance, in the data shown in Fig. 2(b), the horizontal stripes are clearly visible in the contour plot of $\Delta S(q, t)_{PEPC}$, whereas not in the corresponding plot of $\Delta S(q, t)_{exp}$. However, we noticed that the horizontal stripes observed in the contour plot of $\Delta S(q, t)_{PEPC}$ are not created by the PEPC process, but rather originally existed in the data, $\Delta S(q, t)_{exp}$. This artifact was not created, but just became visible in the contour plot because the overall amplitude of the data was reduced through the PEPC process. To demonstrate this, we first smoothed $\Delta S(q, t)_{PEPC}$ and $\Delta S(q, t)_{exp}$ to generate smoothed curves which have a smooth profile in q-space and thus are free from sharp features due to experimental noise and artifacts such as horizontal stripes (Fig. S2, left panel, black). Specifically, for the smoothing, we applied a Savitzky–Golay filter with a polynomial order of 1 and a window of 25 data points. Afterwards, we extracted the sharp artifact features in $\Delta S(q, t)_{PEPC}$ and $\Delta S(q, t)_{exp}$ by subtracting the smoothed curves from $\Delta S(q, t)_{PEPC}$ and $\Delta S(q, t)_{exp}$. To show that the artifact was not generated or strengthened by the PEPC procedure, we compared the resulting artifact features, $\Delta S(q, t)_{PEPC, art}$ and $\Delta S(q, t)_{exp, art}$

(Fig. S2, right panel, blue and red). The comparisons of $\Delta S(q, t)_{\text{PEPC, art}}$ and $\Delta S(q, t)_{\text{exp, art}}$ directly show whether the artifact, including the horizontal stripes, was generated or strengthened by the PEPC procedure or already existed in the original data. According to the comparisons, as Fig. S2 shows, the amplitude of $\Delta S(q, t)_{\text{PEPC, art}}$ and $\Delta S(q, t)_{\text{exp, art}}$ are almost identical, indicating that the artifact, including the horizontal stripes, was not generated or strengthened via the PEPC procedure.

Regarding the data shown in Fig. 3(a), the horizontal stripes were significantly enhanced by the PEPC procedure. To show this point, we extract artifact features in $\Delta S(q, t)_{\text{synch}}$ and $\Delta S(q, t)_{\text{synch, PEPC}}$ using the same method as in the previous example (Fig. S3). Each of $\Delta S(q, t)_{\text{synch}}$ and $\Delta S(q, t)_{\text{synch, PEPC}}$ was smoothed in q-space to generate smooth curves without sharp features arising from experimental artifacts (Fig. S3, left panel, black). The sharp artifact features were then extracted by subtracting the smoothed curves from $\Delta S(q, t)_{\text{synch}}$ or $\Delta S(q, t)_{\text{synch, PEPC}}$. A comparison of the extracted artifact features (Fig. S3, right panel, $\Delta S(q, t)_{\text{synch, art}}$ (blue) and $\Delta S(q, t)_{\text{synch, PEPC, art}}$ (red)) reveals a significant difference in amplitude between the two features, with $\Delta S(q, t)_{\text{synch, PEPC, art}}$ showing a much larger amplitude than $\Delta S(q, t)_{\text{synch, art}}$. The comparison indicates that the sharp artifact features were strengthened by the PEPC treatment. In particular, the difference in amplitude of the artifact features is more pronounced at earlier time delays, specifically at 300 ps and 10 ns, compared to the later time delay of 300 ns.

However, the increase in the amplitude of the artifact features is not inherent to the PEPC method itself. Rather, it is a result of the poor signal-to-noise ratio (S/N ratio) of the signal components used in PEPC, particularly $\Delta S(q, t = 100 \text{ ps})_{\text{exp}}$. To support this claim, we also examined the PEPC treated data using signal components modified to have high S/N ratios. By demonstrating this, we aimed to show that if signal components with high S/N ratios are used in PEPC, the amplitude of the artifact does not change significantly before and after the PEPC treatment, as exemplified in Fig. S2.

We first generated noise-free signal components by applying a Savitzky–Golay filter with a polynomial order of 1 and a window of 25 data points to the original $(\partial S/\partial T)_\rho$ and $\Delta S(q, t = 100 \text{ ps})_{\text{exp}}$. The PEPC method was then applied using these noise-free signal components, resulting in curves denoted as $\Delta S(q, t)_{\text{synch, PEPC, sm}}$ (Fig. S4, left panel, red). Artifact features were subsequently extracted from both the original $\Delta S(q, t)_{\text{synch}}$ and the newly produced $\Delta S(q, t)_{\text{synch, PEPC, sm}}$. The resulting artifact features are denoted as $\Delta S(q, t)_{\text{synch, art}}$ and $\Delta S(q, t)_{\text{synch, PEPC,}}$

sm, art, respectively (Fig. S4, right panel, blue and red). A comparison of the artifact features reveals that the amplitude of the artifact features in the PEPC-treated signal, obtained with smoothed signal components, is comparable to that in the original data, $\Delta S(q, t)_{\text{synch}}$.

Our analysis indicates that the horizontal-stripes artifact observed in $\Delta S(q, t)_{\text{synch, PEPC}}$ is not a result of any systematic artifact introduced by the PEPC method. Rather, it originates either from the original raw data or from the noise present in the signal components $(\partial S/\partial T)_\rho$ or $\Delta S(q, t = 100 \text{ ps})_{\text{exp}}$ used in the PEPC method. Our findings demonstrate that the PEPC method does not generate specific artifacts, such as horizontal stripes, as long as the signal components from which the kinetic contributions are to be removed have a sufficiently high S/N ratio. Thus, any enhanced artifacts observed on the PEPC-treated curves can be attributed to the inherent noise in the signal component used for PEPC. As mentioned in the main text, the PEPC procedure does not involve any fitting process or chi-square (χ^2) estimation; instead, it utilizes vector calculations to determine the amplitude of the signal components to be subtracted. This method eliminates the possibility of errors associated with fitting procedures. Therefore, any enhanced artifacts observed on the PEPC-treated curves are solely due to inherent noise present in the signal components used in the PEPC method, as we have demonstrated above.

C. Determination of coefficients g_k and h_k during structural analysis

For a given structural candidate for the reaction intermediate, the theoretical SADS, $\text{SADS}_{k, \text{theory}}$ can be calculated by using the following equation:

$$\text{SADS}_{k, \text{theory}}(q) = \Delta S_k(q)_{\text{solute, theory}} + \Delta S_k(q)_{\text{cage, theory}}. \tag{S9}$$

Then, $\text{SADS}_k(q)_{\text{corr}}$ which minimizes the discrepancy between $\text{SADS}_k(q)_{\text{corr}}$ and $\text{SADS}_{k, \text{theory}}(q)$ is generated. The relation between $\text{SADS}_k(q)_{\text{corr}}$ and $\text{SADS}_{k, \text{theory}}(q)$ can be expressed as follows:

$$\begin{aligned}\text{SADS}_{k, \text{theory}}(q) &= \text{SADS}_k(q)_{corr} + X(q) \\ &= \text{SADS}_k(q)_{\text{PEPC}} + g_k \times (\partial S/\partial T)_\rho + h_k \times (\partial S/\partial \rho)_T + X(q)\end{aligned} \tag{S10}$$

where $X(q)$ is the discrepancy between $\text{SADS}_k(q)_{\text{corr}}$ and $\text{SADS}_{k, \text{theory}}(q)$. Optimal g_k and h_k are those minimize the norm of $X(q)$, i.e., $|X(q)|$. While the detailed proof will not be described in here, such optimal g_k and h_k can be calculated in a similar manner to the calculation of $d_{k, T}$ and $d_{k, \rho}$ explained in section "Mathematical background for the decomposition of SADS_k into $\text{SADS}_{k, \parallel}$ and $\text{SADS}_{k, \perp}$" as follows:

$$g_k = (\text{SADS}_{k,\,\text{theory}}(q) - \text{SADS}_k(q)_{\text{PEPC}}) \cdot (\partial S/\partial T)_{\rho,\perp}/|(\partial S/\partial T)_{\rho,\perp}|^2, \tag{S11}$$

$$h_k = (\text{SADS}_{k,\,\text{theory}}(q) - \text{SADS}_k(q)_{\text{PEPC}}) \cdot (\partial S/\partial \rho)_{T,\perp}/|(\partial S/\partial \rho)_{T,\perp}|^2. \tag{S12}$$

We note that numerical methods also can be employed to obtain the optimal g_k and h_k without using vector operations that may seem complex at first glance.[1-3] Using numerical approaches, the least-squares solution of the following system of linear equations can be determined:

$$\text{SADS}_{k,\,\text{theory}}(q) - \text{SADS}_k(q)_{\text{PEPC}} = g_k \times (\partial S/\partial T)_\rho + h_k \times (\partial S/\partial \rho)_T. \tag{S13}$$

It is also worth noting that the optimal values of g_k and h_k, obtained via analytical or numerical means, are those which minimize the sum of the squares of the residuals, as expressed by the term "least-squares". However, for the analysis of TRXL data, it is more common and reliable to minimize the weighted least square, such as χ^2, which takes into account the experimental standard deviation. Thus, obtaining the optimal values of g_k and h_k that minimize χ^2 is ideal. To achieve this, we modify Eqs. (S11–S13) as follows:

$$g_k = (\text{SADS}_{k,\,\text{theory}}(q)' - \text{SADS}_k(q)_{\text{PEPC}}') \cdot (\partial S/\partial T)_{\rho,\perp}'/|(\partial S/\partial T)_{\rho,\perp}'|^2, \tag{S14}$$

$$h_k = (\text{SADS}_{k,\,\text{theory}}(q)' - \text{SADS}_k(q)_{\text{PEPC}}') \cdot (\partial S/\partial \rho)_{T,\perp}'/|(\partial S/\partial \rho)_{T,\perp}'|^2, \tag{S15}$$

$$\text{SADS}_{k,\,\text{theory}}(q)' - \text{SADS}_k(q)_{\text{PEPC}}' = g_k \times (\partial S/\partial T)_\rho' + h_k \times (\partial S/\partial \rho)_T'. \tag{S16}$$

Here, the prime notation indicates that the vectors are scaled by the experimental standard deviation, denoted by $\sigma(q)$, as shown in the following equation:

$$A(q)' = A(q)/\sigma(q). \tag{S17}$$

This approach operates on the principle that by scaling Eq. (S10) with $\sigma(q)$, one can obtain the optimal g_k and h_k values that minimizes $|X(q)'|$, whereas the original g_k and h_k values obtained via Eqs. (S11) and (S12) minimizes $|X(q)|$. The Eq. (S10) scaled with $\sigma(q)$ is expressed as follows:

$$\begin{aligned}
\text{SADS}_{k,\,\text{theory}}(q)' &= \text{SADS}_k(q)_{corr}' + X(q)' \\
&= \text{SADS}_k(q)_{\text{PEPC}}' + g_k \times (\partial S/\partial T)_\rho' + h_k \times (\partial S/\partial \rho)_T' \\
&\quad + X(q)'
\end{aligned} \tag{S18}$$

Then, it can be noticed that by substituting original vectors $\text{SADS}_{k,\,\text{theory}}(q)$, $\text{SADS}_k(q)_{\text{PEPC}}$, $(\partial S/\partial T)_{\rho,\perp}$, and $(\partial S/\partial \rho)_{T,\perp}$ in Eqs. (S11) and (S12) with their scaled counterparts, $\text{SADS}_{k,\,\text{theory}}(q)'$, $\text{SADS}_k(q)_{\text{PEPC}}'$, $(\partial S/\partial T)_{\rho,\perp}'$, and $(\partial S/\partial \rho)_{T,\perp}'$, one can obtain the optimal g_k and h_k

values that minimizes $|X(q)'|$ using the same procedure as in the original least-squares optimization. The resulting equations are Eqs. (S14) and (S15). It is also possible to apply the same scaling to Eq. (S13) to enable the numerical method to find the minimum χ^2 solutions instead of least-squares solutions as shown in Eq. (S16).

Accordingly, the inclusion of the parameters g_k and h_k in the molecular structure optimization using PEPC-treated data does not increase the complexity of the fitting process, as they are not considered independent fitting parameters. Consequently, the structural analysis of a $SADS_k(q)_{PEPC}$ has the same level of complexity as that of the original $SADS_k(q)$ that is not subjected to PEPC. Therefore, the PEPC method facilitates the kinetic analysis of $\Delta S(q, t)_{exp}$ by removing the contribution of the known signal components, without compromising the subsequent structural analysis.

D. Comparison of the PEPC method and the nodal-point method (NP method)

In this study, we introduce the PEPC method, designed to remove the kinetic contributions of the signal components with known shapes in q-space from $\Delta S(q, t)_{exp}$. As an example, we demonstrate the removal of the kinetic contribution of $\Delta S(q, t)_{solvent}$, which represents the hydrodynamic response of bulk solvent, using the PEPC method. This removal leaves only the kinetics of $\Delta S(q, t)_{sol-rel}$ in the resulting PEPC-treated signal $\Delta S(q, t)_{PEPC}$, making the analysis of solute kinetics more straightforward.

It should be noted that a conventional method, called the "nodal-point method (NP method)", can offer similar benefits to the PEPC method in some cases. In the NP method, the kinetics of $\Delta S(q, t)_{sol-rel}$ can be determined by monitoring changes in signal intensities at selected q-points, called "nodal points", where the signal intensity of $\Delta S(q, t)_{solvent}$ is zero. Since the intensity of $\Delta S(q, t)_{solvent}$ is zero at these points, the kinetics of $\Delta S(q, t)_{solvent}$ do not contribute to the signal intensities at the nodal points. Thus, any rise and decay of signal intensities at the nodal points can be attributed to the kinetics of $\Delta S(q, t)_{sol-rel}$.

This NP method may seem intuitive and straightforward, but it suffers from two significant limitations related to accuracy and applicability. For example, to use the NP method for removing the kinetic contributions of $\Delta S(q, t)_{solvent}$, nodal points for $\Delta S(q, t)_{solvent}$ are required. However, $\Delta S(q, t)_{solvent}$ is a linear combination of two different components, $(\partial S/\partial T)_\rho$ and $(\partial S/\partial \rho)_T$, and the positions of nodal points for these two components differ in general. Thus,

the position where the intensity of $\Delta S(q, t)_{solvent}$ is zero varies depending on the relative ratio of $(\partial S/\partial T)_\rho$ and $(\partial S/\partial \rho)_T$, as shown in Fig. S9(b). This example illustrates that the requirement for nodal points significantly restricts the applicability of the NP method, making it unable to eliminate the kinetic contributions of multiple trivial components. We stress that, in contrast, the PEPC method is widely applicable and not subject to such limitations, as demonstrated in sections II H and II I of the main text.

In addition to the aforementioned limitations, the NP method also has limitations in terms of accuracy. Specifically, the NP method relies solely on signal intensities at the nodal points, thereby restricting its precision in extracting solute kinetics. In contrast, the PEPC method utilizes signals from all q-points, resulting in smaller errors associated with kinetic analysis, even in scenarios where the NP method is applicable. To demonstrate this point, we compared the kinetic analysis results obtained using the NP method, PEPC method, and global fitting analysis (GFA). We applied the NP method to $\Delta S(q, t)_{exp}$ for $[Au(CN)_2^-]_3$ in water presented in Fig. 2(b). The solvent term typically consists of two signal components, $(\partial S/\partial T)_\rho$ and $(\partial S/\partial \rho)_T$, as Eq. (8) shows. However, in this case, only $(\partial S/\partial T)_\rho$ was considered, as our previous work[4] has shown that $(\partial S/\partial T)_\rho$ and $(\partial S/\partial \rho)_T$ have similar shapes for water. Consequently, $(\partial S/\partial T)_\rho$, $(\partial S/\partial \rho)_T$ and $\Delta S(q, t)_{solvent}$, which is a linear combination of the formal two components, share the same nodal points. As shown in Fig. S9(a), $(\partial S/\partial T)_\rho$ of water has 11 nodal points in the q-range of $1.0 - 6.5$ ($q = 1.5, 2.1, 2.8, 3.7, 4.2, 4.4, 4.6, 4.7, 4.9, 5.6,$ and 5.9 Å^{-1}). By applying the NP method, solute kinetics were extracted by analyzing the time profiles of $\Delta S(q, t)_{exp}$ at these 11 nodal points. Specifically, the profiles of $\Delta S(q, t)_{exp}$ at the nodal points were globally fitted as a convolution of an instrument response function (IRF) of ~480 fs FWHM with a sum of exponential rise and decay functions sharing common time constants. The kinetic analysis revealed three time constants (2.2 ± 0.5 ps, 185 ± 71 ps, and 100 ± 24 ns), as shown in Fig. S9.

The obtained time constant values of 2.2 ps, 185 ps, and 100 ns displayed notable deviations from those determined using the PEPC method, which were 1.7 ps, 1.0 ns, and 114 ns, respectively. They also deviated from the constants obtained through the GFA method, which were 1.6 ps, 3.0 ns, and 100 ns, respectively. Additionally, the relative error of the time constant values obtained using the NP method (27%, 38%, and 24% for the obtained time constants of 2.2 ps, 185 ps, and 100 ns, respectively) was substantially higher than the relative errors from PEPC (6%, 10%, and 2.6%) or GFA (6%, 17%, and 20%). This large error from the NP method

is expected as it relies solely on information obtained from the limited number of nodal points (11 nodal points out of a total of 1,100 q-points for the data shown in the example). Due to the limited information, the accuracy of the analysis is relatively low. Due to the inherent inaccuracies, the NP method is typically unsuitable for rigorous kinetic analysis of experimental data and has mainly been used for on-the-fly monitoring of kinetics observed in the data being collected during experiments. Taken together with the limited applicability of the NP method, the comparison demonstrates that the PEPC method represents a significant advancement in the analysis of the signals obtained from TRXL experiments.

II. Supplementary Figures
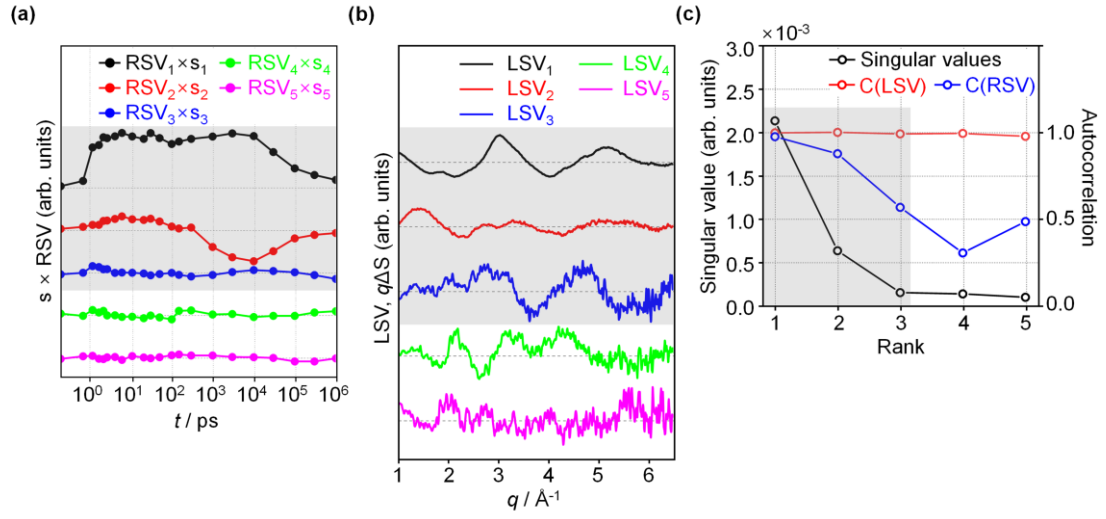
FIG. S1. Singular value decomposition (SVD) analysis of $\Delta S(q, t)_{\text{PEPC}}$ shown in Fig. 2(b). (a) First five right singular vectors (RSVs) weighted by their corresponding singular values. (b) First five left singular vectors (LSVs). (c) Singular values, and the autocorrelation values for RSVs and LSVs from (a) and (b), respectively. The singular values and autocorrelation values, together with the shape of the RSVs, suggest that up to three significant components contribute to the signal. The significant LSVs and RSVs, along with their corresponding singular and autocorrelation values, are highlighted in gray.
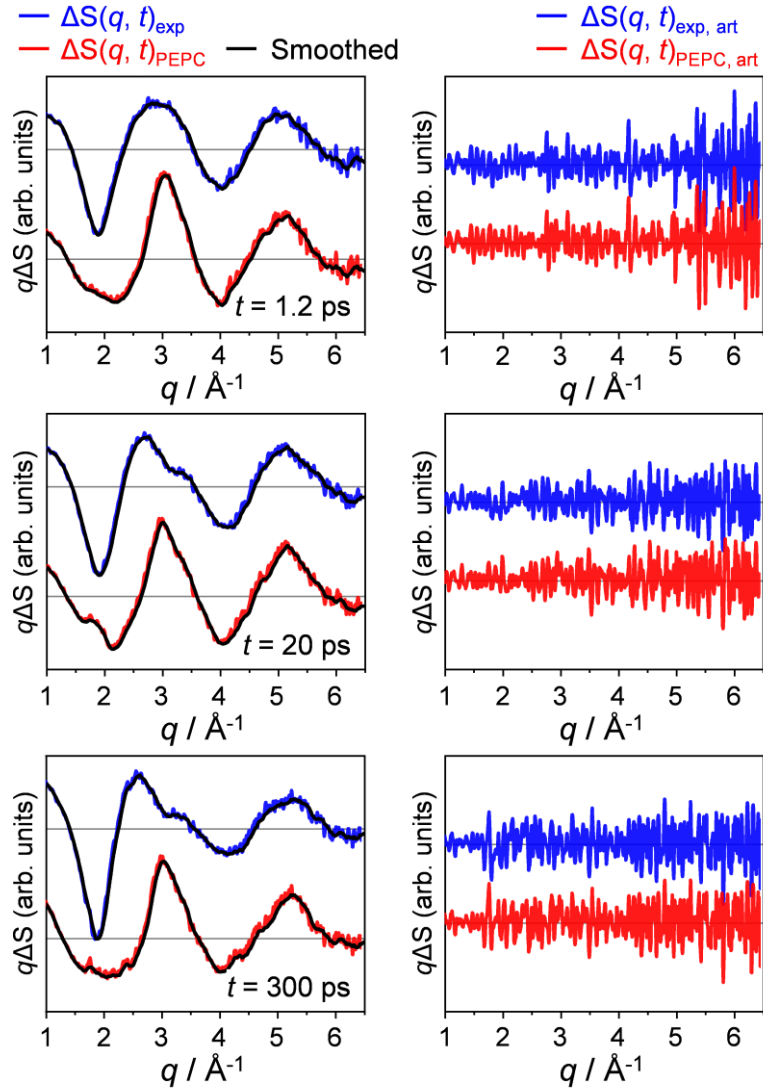
FIG. S2. Comparison of the experimental artifacts (and noise) in the TRXL data before and after PEPC treatment. Experimental artifacts were extracted and compared for $\Delta S(q, t)_{exp}$ and $\Delta S(q, t)_{PEPC}$ obtained from $[Au(CN)_2^-]_3$ dissolved in water (Fig. 2(b)). To extract the experimental artifacts from $\Delta S(q, t)_{exp}$ and $\Delta S(q, t)_{PEPC}$, each of $\Delta S(q, t)_{exp}$ and $\Delta S(q, t)_{PEPC}$ was smoothed in q-space to generate a curve without sharp features arising from the experimental artifacts (left panel, black). The sharp artifact features were then extracted by subtracting the smoothed curve from $\Delta S(q, t)_{exp}$ or $\Delta S(q, t)_{PEPC}$. A comparison of the sharp artifact features from $\Delta S(q, t)_{exp}$ ($\Delta S(q, t)_{exp, art}$, right panel, blue) and $\Delta S(q, t)_{PEPC}$ ($\Delta S(q, t)_{PEPC, art}$, right panel, red) shows that the shape and amplitude of sharp features remain almost unchanged before and after PEPC treatment. The comparison is shown for three representative time delays: 1.2 ps, 20 ps, and 300 ps.
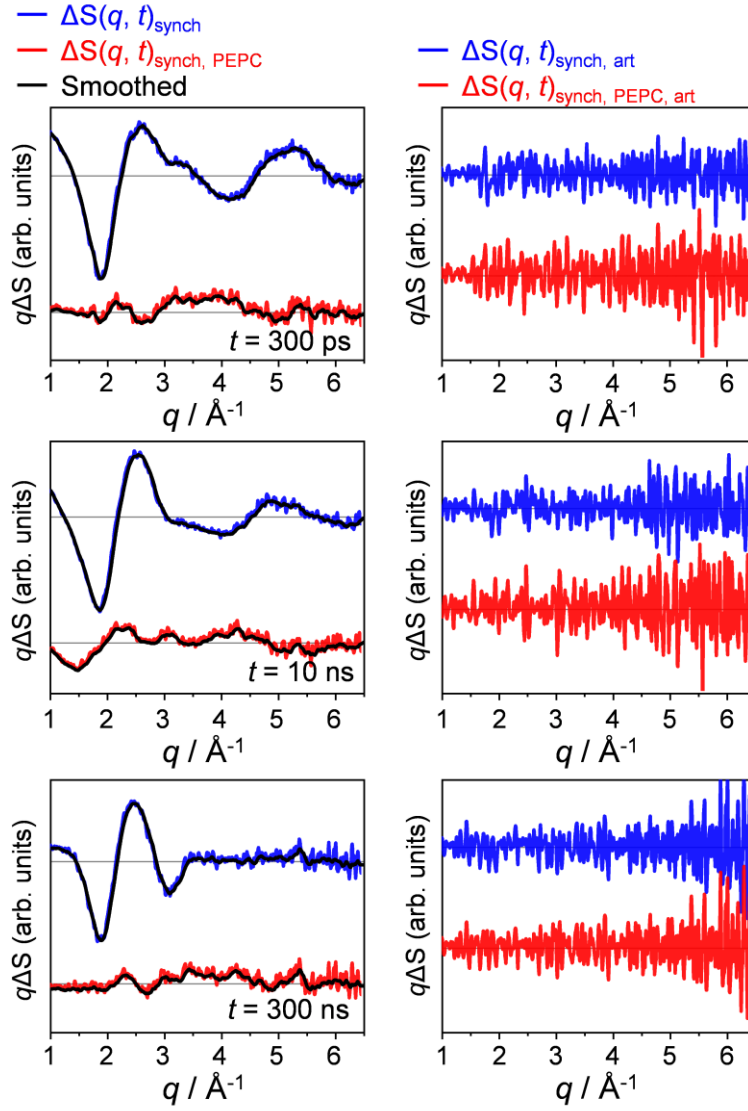
FIG. S3. Comparison of the experimental artifacts (and noise) in the TRXL data before and after PEPC treatment. The artifact features were extracted and compared for $\Delta S(q, t)_{synch}$ and $\Delta S(q, t)_{synch, PEPC}$ obtained from [Au(CN)$_2^-$]$_3$ dissolved in water (Fig. 3(a)). The contributions of $(\partial S/\partial T)_\rho$ from the water solvent and $\Delta S(q, t = 100 \text{ ps})_{exp}$ were removed via the PEPC treatment. The same method used to extract artifact features in Fig. S2 was employed. Each of $\Delta S(q, t)_{synch}$ and $\Delta S(q, t)_{synch, PEPC}$ was smoothed in q-space to generate a smooth curve without sharp features arising from experimental artifacts (left panel, black). The sharp artifact features were then extracted by subtracting the smoothed curve from $\Delta S(q, t)_{synch}$ or $\Delta S(q, t)_{synch, PEPC}$. Comparison of the extracted artifact features (right panel, $\Delta S(q, t)_{synch, art}$ and $\Delta S(q, t)_{synch, PEPC, art}$) reveals a significant difference in amplitude between the two features, with $\Delta S(q, t)_{synch, PEPC, art}$ showing much larger amplitude than $\Delta S(q, t)_{synch, art}$. The comparison indicates that the sharp artifact features were strengthened by the PEPC treatment. The comparison is shown for three representative time delays: 300 ps, 10 ns, and 300 ns.
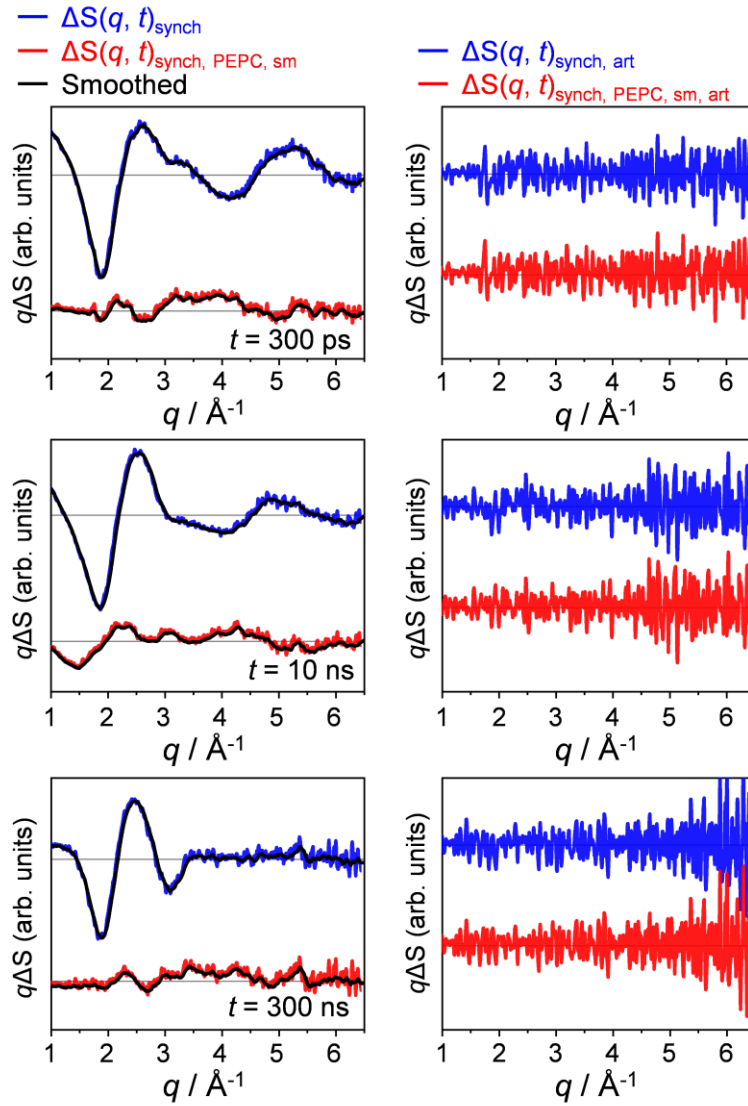
FIG. S4. Comparison of the experimental artifacts (and noise) in the TRXL data before and after PEPC treatment. In contrast to the data shown in Fig. 3(a), where the components $(\partial S/\partial T)_\rho$ from water solvent and $\Delta S(q, t = 100 \text{ ps})_{exp}$ were used as is, the two components were smoothed to remove the artifact features prior to the PEPC treatment. The resulting curves are denoted as $\Delta S(q, t)_{synch, PEPC, sm}$. Artifact features were then extracted using the same method used to extract artifact features in Fig. S2. Each of $\Delta S(q, t)_{synch}$ and $\Delta S(q, t)_{synch, PEPC, sm}$ was smoothed in q-space to generate a smooth curve without sharp features arising from experimental artifacts (left panel, black). The sharp artifact features were then extracted by subtracting the smoothed curve from $\Delta S(q, t)_{synch}$ or $\Delta S(q, t)_{synch, PEPC, sm}$. The comparison (right panel, $\Delta S(q, t)_{synch, art}$ and $\Delta S(q, t)_{synch, PEPC, sm, art}$) shows that the amplitudes of the artifact features in $\Delta S(q, t)_{synch}$ and $\Delta S(q, t)_{synch, PEPC, sm}$ are almost identical, demonstrating that the PEPC process does not create or enhance artifacts in the data when using signal components with a high signal-to-noise ratio, i.e., the components that do not contain sharp artifacts. The comparison is shown for three representative time delays: 300 ps, 10 ns, and 300 ns.
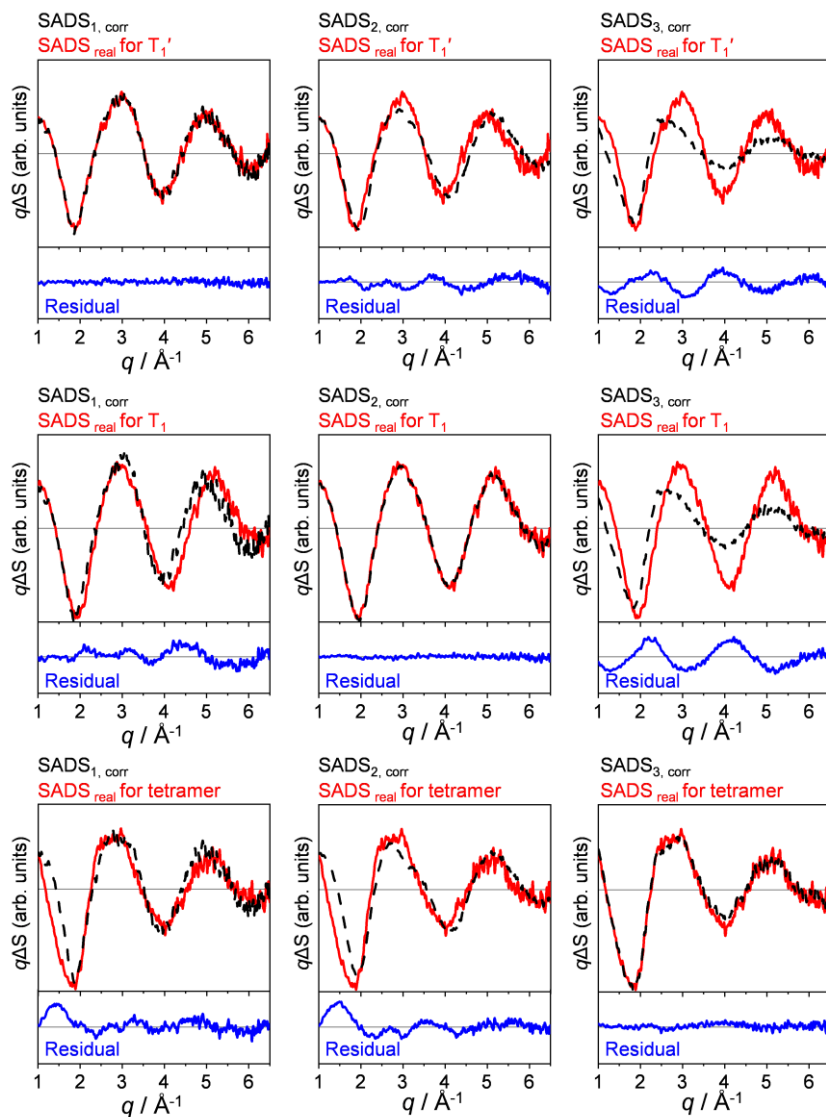
FIG. S5. Comparisons between SADS$_{real}$ and the corresponding SADS$_{k, corr}$ for three different molecular structures of reaction intermediates. Each of the three SADS$_{real}$'s corresponds to T$_1'$, T$_1$, and tetramer shown in Fig. 2(a), respectively. We calculated SADS$_{k, corr}$ for each k by correcting SADS$_{k, PEPC}$ to minimize the discrepancy between SADS$_{k, corr}$ and SADS$_{real}$. The resulting SADS$_{real}$'s and SADS$_{k, corr}$'s are plotted together, and the residual (SADS$_{k, corr}$ - SADS$_{real}$) is also plotted to visualize the degree of agreement between the two. The comparison shows that the SADS$_{k, corr}$ for a given k matches only with the SADS$_{real}$ for the correct molecular structure of intermediate. For instance, SADS$_{1, corr}$ matches only with SADS$_{real}$ for T$_1'$ and shows a significant discrepancy with SADS$_{real}$'s for T$_1$ or the tetramer.

S14

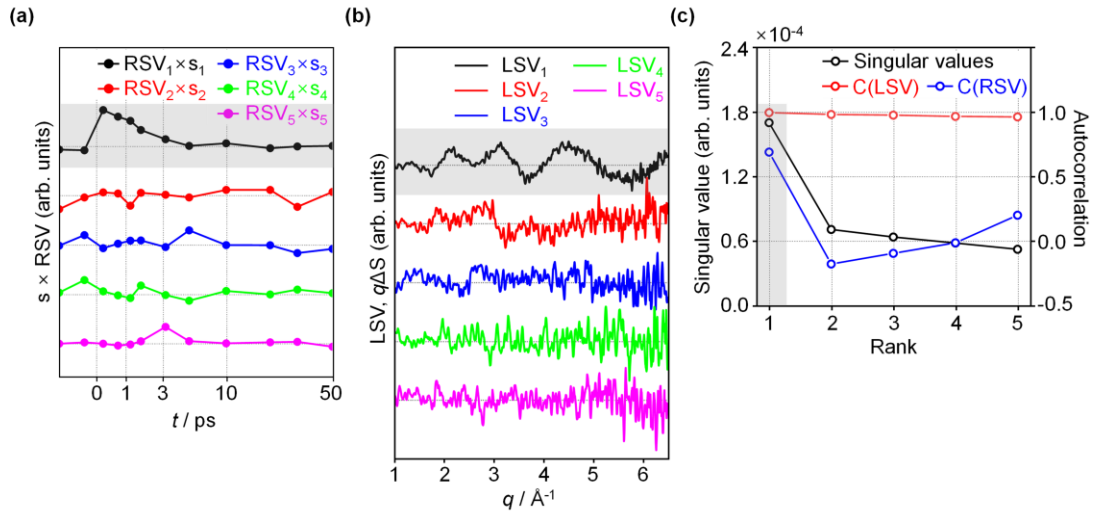FIG. S6. SVD analysis of $\Delta S(q, t)_{XFEL, PEPC}$ shown in Fig. 3(a). (a) First five RSVs weighted by their corresponding singular values. (b) First five LSVs. (c) Singular values, and the autocorrelation values for RSVs and LSVs from (a) and (b), respectively. The singular values and autocorrelation values, together with the shape of the RSVs, suggest that only a single significant component contributes to the signal. The significant LSV and RSV, along with its corresponding singular and autocorrelation value, are highlighted in gray.
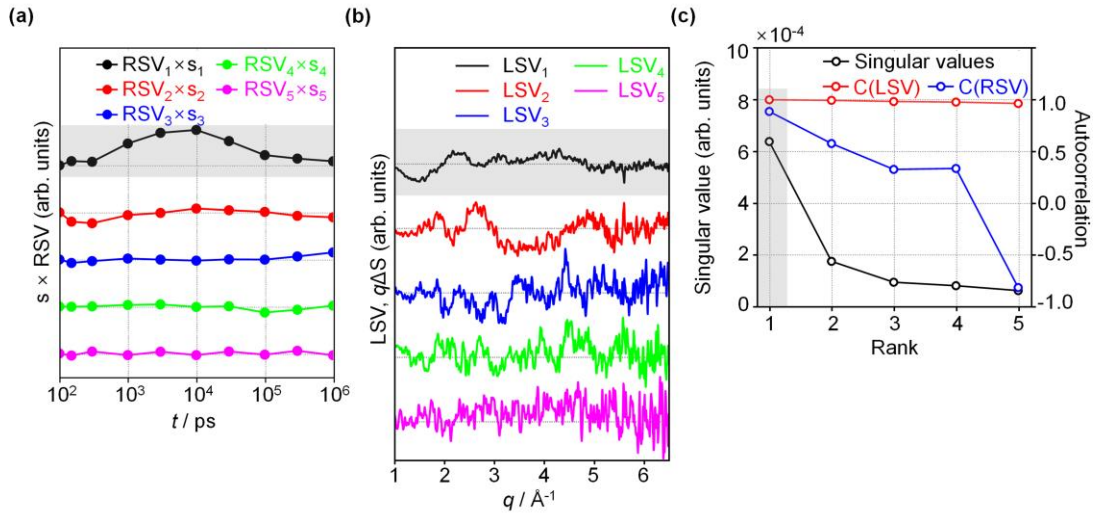
S15

FIG. S7. SVD analysis of $\Delta S(q, t)_{\text{synch, PEPC}}$ shown in Fig. 3(a). (a) First five RSVs weighted by their corresponding singular values. (b) First five LSVs. (c) Singular values, and the autocorrelation values for RSVs and LSVs from (a) and (b), respectively. The singular values and autocorrelation values, together with the shape of the RSVs, suggest that only a single significant component contributes to the signal. The significant LSV and RSV, along with its corresponding singular and autocorrelation value, are highlighted in gray.
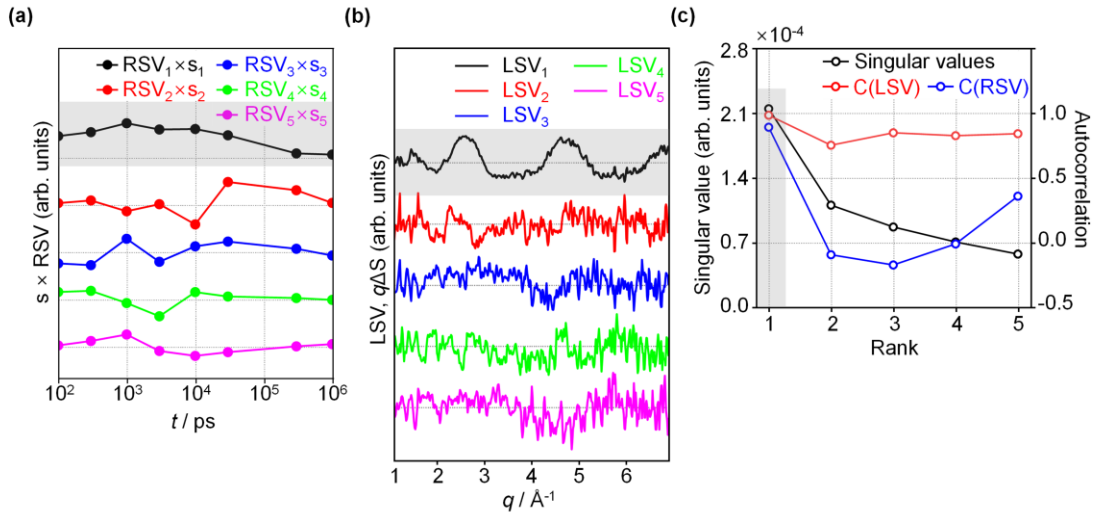
FIG. S8. SVD analysis of $\Delta S(q, t)_{PEPC}$ shown in Fig. 4(c). (a) First five RSVs weighted by their corresponding singular values. (b) First five LSVs. (c) Singular values, and the autocorrelation values for RSVs and LSVs from (a) and (b), respectively. The singular values and autocorrelation values, together with the shape of the RSVs, suggest that only a single significant component contributes to the signal. The significant LSV and RSV, along with its corresponding singular and autocorrelation value, are highlighted in gray.
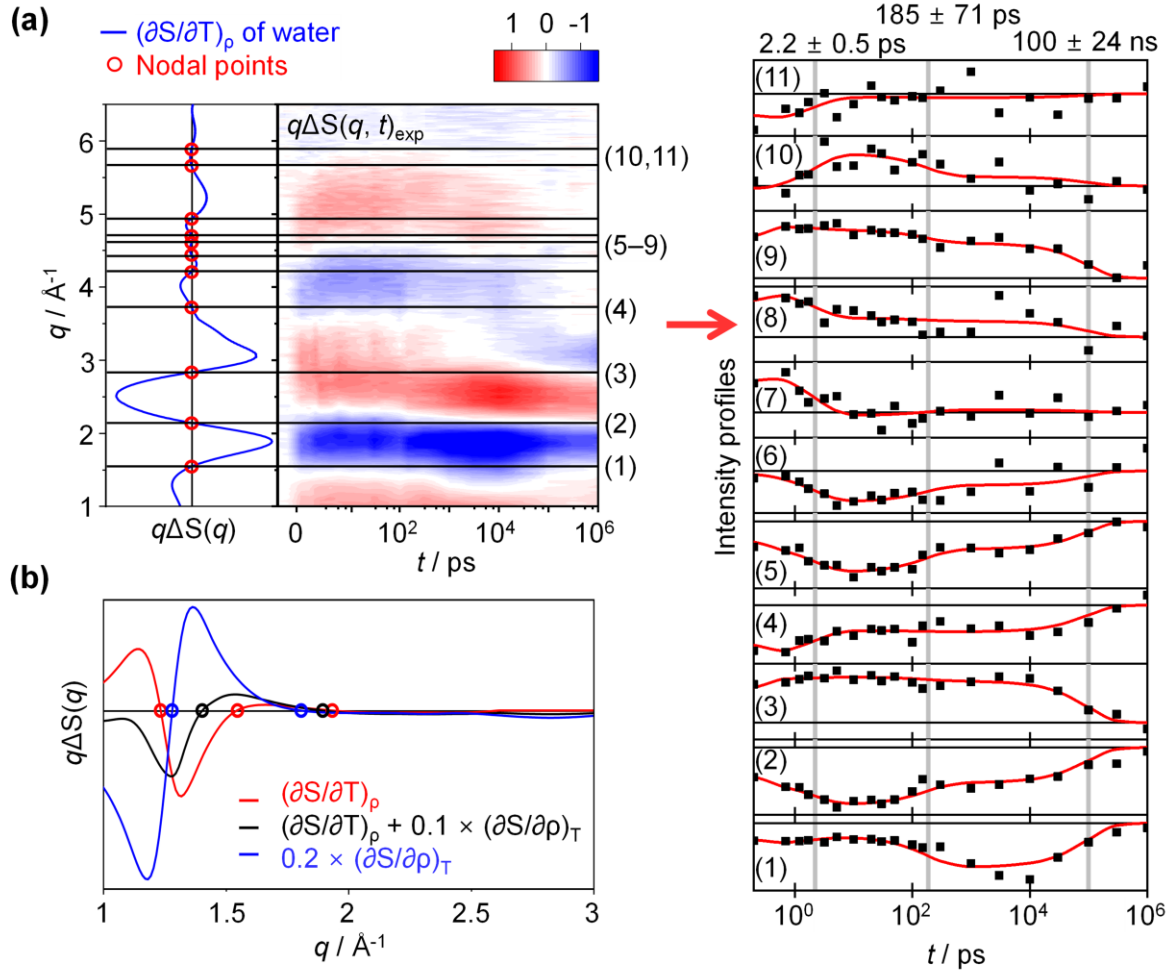
FIG. S9. Demonstration of the conventional nodal-point (NP) method for eliminating kinetic contributions in TRXL data. (a) Application of NP method to $\Delta S(q, t)_{exp}$ shown in Fig. 2(b). We aimed to eliminate the kinetic contribution of $(\partial S/\partial T)_\rho$ of water by selecting 11 nodal points in the q-range of $1.0 - 6.5$ Å^{-1}. The time-dependent intensity profiles of $\Delta S(q, t)_{exp}$ at the 11 nodal points are shown in the right panel. The kinetic analysis of the time profiles revealed three time constants (2.2 ± 0.5 ps, 185 ± 71 ps, and 100 ± 24 ns). (b) $\Delta S(q, t)_{solvent}$ of cyclohexane. The positions of zero-crossing points, the q-points where $\Delta S(q, t)_{solvent} = 0$, depend on the relative ratio of $(\partial S/\partial T)_\rho$ and $(\partial S/\partial \rho)_T$, leading to the absence of the nodal points for $\Delta S(q, t)_{solvent}$ of cyclohexane. Consequently, the NP method cannot be used to eliminate the kinetic contributions of $\Delta S(q, t)_{solvent}$ from the TRXL data for solvents like cyclohexane.

III. Supplementary References

[1] C. D. Meyer, *Matrix analysis and applied linear algebra* (Siam, 2000), p.439.

[2] N. J. Salkind, *Encyclopedia of measurement and statistics* (SAGE publications, 2006), p.530-536.

[3] L. Hogben, *Handbook of linear algebra* (CRC press, 2007), p.86.

[4] K. H. Kim, J. G. Kim, S. Nozawa, T. Sato, K. Y. Oang, T. W. Kim, H. Ki, J. Jo, S. Park, C. Song, T. Sato, K. Ogawa, T. Togashi, K. Tono, M. Yabashi, T. Ishikawa, J. Kim, R. Ryoo, J. Kim, H. Ihee, and S. Adachi, "Direct observation of bond formation in solution with femtosecond X-ray scattering," Nature **518**, 385-389 (2015).